MHD STAGNATION POINT FLOW OF MICROPOLAR FLUIDS TOWARDS A STRETCHING SHEET

Sajjad Hussain[1,a], M. Anwar Kamal[2] , F. Ahmad[3] and M. Shafique[4]

s.nawaz@mu.edu.sa[1], makamal@yahoo.com[2], f.ishaq@mu.edu.sa[3], msafique6161@hotmail.com[4]

[1, 3] Mathematics Department, Majmaah University, College of Sciences, Alzulfi, KSA

a: Correspondence author, sajjad_h96@yahoo.com

[2] Department of Mathematics, Suleman Bin Abdul Aziz University Al-Kharj, KSA

[4]Presently:70 Stevenvale, Toronto, Ontario, Canada

ABSTRACT: MHD stagnation point flow of micropolar fluids towards a stretching sheet is studied in the presence of variable surface temperature. The governing partial differential equations of motion are transformed to ordinary differential equations using appropriate similarity transformations. The resulting ordinary differential equations are solved numerically using SOR method and Simpson's (1/3) rule. The numerical results are improved by Richardson's extrapolation. The effects of Magnetic parameter M, velocity ratio parameter λ , Prandtl number P_r and temperature index parameter n are investigated on the features of the velocity and temperature profiles. Comparison of micropolar fluids with Newtonian fluids is presented.

AMS Subject Classification: 76M20.

Key Words: Micropolar fluids, MHD stagnation point flow, Stretching sheet, Prandtl number, Richardson's extrapolation.

1. INTRODUCTION

The dynamics of micropolar fluids has been an expanding research field since introduced by Eringen [1, 2]. Several researchers have made extensive theoretical and experimental investigations for micropolar fluid flows in the presence of transverse magnetic field. The exact solutions for the steady MHD stagnation point flow towards a stretching surface for micropolar fluids were obtained by Mahapatra and Gupta [3]. The effect of the magnetic field on the flow of a micropolar fluid past a continuously moving plate has been studied by Seddeek [4]. Rehman et al. [5] considered heat transfer in two-dimensional steady hyderomagnetic natural convection flow of a micropolar fluid past a non-linear stretching sheet with temperature dependent viscosity. Mohammedein and Gorla [6] analyzed the flow of micropolar fluids bounded by a stretching sheet with a prescribed wall heat flux, viscous dissipation and internal heat generation. Kamal and Hussain [7] studied the three dimensional micropolar fluid motion caused by the stretching surface. Lok et al. [8] investigated non orthogonal stagnation point flow of a micropolar fluid.

The importance of the stagnation point flow is due to its wide applications such as cooling of electronic devices by fans, cooling of nuclear reactors, and many hydrodynamic processes and hence attracted attention of many researchers. Kumari and Nath [9] studied micropolar fluid flow at stagnation point of two dimensional as well as axisymmetric problems. The heat transfer and fluid flow on a stretching surface plays an important role in polymer industry and other engineering fields. Ashraf et al. [10] presented numerical study for the steady, two-dimensional, laminar and incompressible flow of a micropolar fluid in a porous channel.

Ishak et al. [11] studied mixed convection stagnation point flow of a micropolar fluid towards a stretching sheet. Ishak et al. [17] investigated magnetohydrodynamic (MHD) flow of a micropolar fluid towards a stagnation point on a vertical surface. Hayat et al. [18] considered the effects of radiation and magnetic field on the mixed convection stagnation point flow over a vertical stretching sheet in a porous medium. Hayat et al. [19] studied the MHD flow of a micropolar fluid near a stagnation point towards a non-linear stretching surface. Sajjad and Kamal [20] studied boundary layer flow for micropolar electrically conducting fluid on a rotating disk in the presence of magnetic field.

This work looks into numerical solution of MHD stagnation point flow of micropolar fluids towards a stretching sheet in the presence of variable surface temperature. The effects of parameters involved in the study have been observed in detail and presented in tabular and graphical forms.

2. MATHEMATICAL ANALYSIS

Fluid flow is considered to be steady, two dimensional, incompressible and electrically conducting near the stagnation point on a stretching sheet. The Cartesian coordinates system is being used. The stretching velocity is $U_w(\mathrm{x})$ and $U_\infty(\mathrm{x})$ is the free stream velocity, both are being considered proportional to x , the distance from stagnation point. $U_w(\mathrm{x}) = a\mathrm{x}$, $U_\infty(\mathrm{x}) = b\mathrm{x}$ where *a*, *b* are constants such that $a > 0$ and $b \geq 0$. The temperature of the fluid at the surface of the sheet is $T_w(x) = T_\infty + cx^n$. Here c and n are constants with $c>0$ stands for heated surface and T_∞ is ambient fluid

temperature. A uniform magnetic field of strength B_0 is applied in the positive y-direction normal to the stretching sheet. The magnetic Reynolds number is small and the induced magnetic field is negligible. We also assume that the body couples and energy dissipation are neglected.

Under these assumptions the basic equations of motion Eringen [2] become:

$$\frac{\partial u}{\partial x}+\frac{\partial v}{\partial y}=0 \qquad (1)$$

$$(\mu+\kappa)\left(\frac{\partial^2 u}{\partial x^2}+\frac{\partial^2 u}{\partial y^2}\right)+\kappa\left(\frac{\partial \upsilon_3}{\partial y}\right)-\frac{\partial p}{\partial x}=\rho\left(u\frac{\partial u}{\partial x}+v\frac{\partial u}{\partial y}\right) \qquad (2)$$

$$(\mu+\kappa)\left(\frac{\partial^2 v}{\partial x^2}+\frac{\partial^2 v}{\partial y^2}\right)-\kappa\left(\frac{\partial \upsilon_3}{\partial x}\right)-\frac{\partial p}{\partial y}+\underline{J}\times\underline{B}=\rho\left(u\frac{\partial v}{\partial x}+v\frac{\partial v}{\partial y}\right) \qquad (3)$$

$$-\gamma\left(\frac{\partial^2 \upsilon_3}{\partial x^2}+\frac{\partial^2 \upsilon_3}{\partial y^2}\right)+\kappa\left(\frac{\partial v}{\partial x}-\frac{\partial v}{\partial y}\right)-2\kappa\upsilon_3=\rho j\left(u\frac{\partial \upsilon_3}{\partial x}+v\frac{\partial \upsilon_3}{\partial y}\right) \qquad (4)$$

$$u\frac{\partial T}{\partial x}+v\frac{\partial T}{\partial y}=\alpha\left(\frac{\partial^2 T}{\partial y^2}\right) \qquad (5)$$

where ρ is the density, $\underline{V}=V(u,v,0)$, the velocity vector, $\underline{\upsilon}=\upsilon(0,0,\upsilon_3)$, the micro-rotation or spin, p the pressure, j the micro-inertia, γ, μ and κ are material constants, T is fluid temperature, v and α are kinematic viscosity and thermal diffusivity, respectively and the relation for electromagnetic body force as given by Rossow[21] is $\underline{J}\times\underline{B}=\underline{E}\sigma(\underline{V}\times\underline{B})\times\underline{B}=-\sigma B^2\underline{V}$

The boundary conditions are

$$\left.\begin{aligned} &y=0, u=U_W(x), v=0, \underline{\upsilon}=0, T=T_W(x)\\ &y\to\infty, u=U_\infty(x), \underline{\upsilon}=0, T=T_\infty\end{aligned}\right\} \qquad (6)$$

Using the following similarity transformations:

$$\left.\begin{aligned} &u=axf'(\eta), v=-\sqrt{av}\,xf(\eta),\\ &\theta(\eta)=\frac{T-T_\infty}{T_W-T_\infty}, \upsilon_3=-ax\sqrt{\frac{a}{v}}L(\eta)\end{aligned}\right\} \qquad (7)$$

where $\eta=\sqrt{\frac{a}{v}}y$ is dimensionless variable, the continuity equation is satisfied identically and equations (2) to (5) are transformed in to following ordinary differential equations:

$$\left.\begin{aligned} &(1+C_1)f'''+ff''-f'^2+\lambda^2+\\ &M(\lambda-f')-C_1L'=0\end{aligned}\right\} \qquad (8)$$

$$C_3L''+C_1C_2f''-C_1C_2L=Lf'-fL' \qquad (9)$$

$$\theta''+\Pr(f\theta'-nf'\theta)=0, \qquad (10)$$

with the corresponding boundary conditions:

$$\left.\begin{aligned} &\eta=0, \quad f=0, \quad f'=1, \quad L=0, \quad \theta=1\\ &\eta\to\infty, \ f'=\lambda, \quad L=0, \quad \theta=0\end{aligned}\right\} \qquad (11)$$

where prime denotes differentiation with respect to η and $\lambda=\frac{b}{a}$, $\Pr=\frac{v}{\alpha}$, $M=\frac{\sigma B^2 0}{\rho a}$ are velocity ratio parameter, Prandtl number and the magnetic parameter respectively.The constants $C_1=\frac{\kappa}{\mu}, C_2=\frac{\gamma}{\mu j}$ and $C_3=\frac{\kappa}{\rho j a}$ are dimensionless.

3. FINITE DIFFERENCE EQUATIONS

In order to obtain the numerical solutions, let

$$f'=q \qquad (12)$$

and then the equations (8) to (10) take the form as:

$$\left.\begin{aligned} &(1+C_1)q''+fq'-q^2+\lambda^2\\ &+M(\lambda-q)-C_1L'=0\end{aligned}\right\} \qquad (13)$$

$$C_3L''+C_1C_2(q'-L)=Lq-fL' \qquad (14)$$

$$\theta''+\Pr(f\theta'-nq\theta)=0 \qquad (15)$$

with the boundary conditions:

$$\left.\begin{aligned} &\eta = 0, \quad f = 0, \quad q = 1, \quad L = 0, \quad \theta = 1 \\ &\eta \to \infty, q = \lambda, \quad L = 0, \quad \theta = 0 \end{aligned}\right\} \quad (16)$$

By using the central difference approximation to the derivatives involved in the equation (13) to (15) at a typical point $\eta=\eta_n$ of the interval [0, t] where t is sufficiently large, we obtain

$$\left.\begin{aligned} &(2(1+C_1)+hf_n)q_{n+1}+(2(1+C_1)-hf_n)q_{n-1} \\ &-(4(1+C_1)+2h^2M+2h^2q_n)q_n+2h^2M\lambda \\ &+2h^2\lambda^2-C_1h(L_{n+1}-L_{n-1})=0 \end{aligned}\right\} \quad (17)$$

$$\left.\begin{aligned} &(2C_3+hf_n)L_{n+1}+(2C_3-hf_n)L_{n-1} \\ &-(4C_3+2h^2C_1C_2-2h^2q_n)L_n \\ &+hC_1C_2(q_{n+1}-q_{n-1})=0 \end{aligned}\right\} \quad (18)$$

$$\left.\begin{aligned} &(\frac{2}{P_r}-hf_n)\theta_{n+1}-(\frac{4}{P_r}+2h^2\eta q_n)\theta_n \\ &+(\frac{2}{P_r}-hf_n)\theta_{n-1}=0 \end{aligned}\right\} \quad (19)$$

where h denotes a grid size. Also the symbols used denote $q_n = q(\eta_n)$ and $f_n = f(\eta_n)$ and $\theta_n = \theta(\eta_n)$ etc.

4. COMPUTATIONAL PROCEDURE

The finite difference equations (17) to (19) are solved by using SOR method Smith [13] and the equation (12) is integrated using Simpson's (1/3) rule Gerald [14] with the formula Milne [15, p.48] subject to the appropriate boundary conditions.

The order of the sequence of iterations is as follows:

1. The equations (17) to (19) for the solution of *q*, *L* and θ are solved subject to the boundary conditions:

$q = 1, \quad \theta = 1, \quad L = 0$ when $\eta = 0$

$q \to \lambda, \quad \theta \to 0, \quad L \to 0$ when $\eta \to \infty$

2. The computed solutions of *q* are then introduced in to equation (12) which is then integrated using the initial condition $f(0) = 0$ to obtain the solution for *f*.

3. The optimum value of the relaxation parameter ω_{opt} is estimated to accelerate the convergence of the SOR method.

4. The SOR procedure is terminated when the following criterion is satisfied: $\max \left| U_i^{m+1} - U_i^m \right| < 10^{-6}$ where *m* denotes the number of iterations and *U* stands for each of q, *L* and θ. The above steps 1 to 4 are repeated for all the grid sizes considered. The solutions of f', *L* and θ are order of accuracy $O(h^2)$ while the solution of equation (12) is of the order of accuracy $O(h^5)$. Higher order accuracy $O(h^6)$ of the numerical results is obtained by Richardson's Extrapolation method Burden [16]. Our numerical scheme is straight forward and very efficient for obtaining the solution and hence extending the ranges of the parameters of the problems. Also, the scheme is more economical and easy to program.

5. RESULTS AND DISCUSSION

Case	C_1	C_2	C_3
I	0.05	1.5	2.0
II	1.5	2.5	3.0
III	4.0	5.0	6.0

The effects of the parameters namely *M*, λ, P_r and n for the ranges $0 \le M \le 20$, $0 \le \lambda \le 4$, $0 \le \Pr \le 8$ and $0 \le n \le 3$ respectively are observed on velocity, microrotation and temperature distributions and the results are presented in the tabular as well as in graphical forms. The calculations are made on three different grid sizes namely *h*= 0.05, 0.025 and 0.0125 for three different sets of the material constants C_1, C_2 and C_3.

The results are presented for the non-dimensional velocity components f, f', microrotation function *L* and temperature function θ in tables 1 and 2 corresponding to case-I of the material constants. Also, the results of the functions f' and θ in the higher order of accuracy $O(h^6)$ are given in tables 3 to 4 in the case - I.

Table 5 shows that the magnitude of the skin friction coefficient $f''(0)$ increases with increasing values of the magnetic parameter *M* whether λ >1or λ < 1 but the magnitude of $f''(0)$ decreases for micropolar fluids in comparison with Newtonian fluids. Also, the magnitude of skin friction coefficient $f''(0)$ decreases for increasing values of material constants C_1, C_2 and C_3 as

shown in table 6.The heat transfer rate at the surface $-\theta'(0)$ known as the local Nusselt number increases with the increasing values of the parameters P_r , λ, n as shown in the table 7. When λ >1, the magnetic parameter *M* has increasing effect on $-\theta'(0)$. While for λ <1, *M* has a decreasing effect on $-\theta'(0)$ as presented in the table 8.

Fig. 1 depicts that the velocity profile f' increases for some values of η and then becomes uniform when the stretching velocity ax is less than the external stream velocity bx i.e. λ >1. In fact, it shows the behavior boundary layer and the boundary layer thickness decreases with increasing *M*. In case, the fluid and the surface move with equal velocities i.e. $\lambda = 1$, the magnetic parameter *M* has no effect on the velocity field and hence the velocity profiles coincide for different values of *M*. and the magnitude of the skin friction coefficient $f''(0)$ remains zero. When the value of stretching velocity ax is greater than that of external stream velocity bx i.e. λ <1, the velocity profile f' shows an inverted boundary layer behavior and the boundary layer thickness decreases with increasing values of *M* .

The temperature distribution $\theta(\eta)$ decreases to zero with increasing η . The increasing values of the parameters P_r , λ, n have increasing effect on the temperature gradient at the surface because the thermal boundary layer decreases by increasing these parameters. These results have been shown in figures 2 to 5. The comparison of f' for Newtonian and micropolar fluids is shown in fig.6 and fig.7. The fig.8 and fig.9 depict the microrotation *L*.

Table 1 (a) : Numerical results using SOR Method and Simpson's(1/3) Rule for finer grid size

M=0.0, λ =2.0, P_r =1.0, n=1.0				
η	f	f'	θ	L
0.000	0.000000	1.000000	1.000000	0.000000
0.400	0.529177	1.581453	0.501051	0.005916
0.800	1.223958	1.853704	0.204211	0.006987
1.200	1.989983	1.958062	0.066391	0.005729
1.600	2.781010	1.990268	0.016895	0.003866
2.000	3.579083	1.998135	0.003312	0.002250
2.400	4.378717	1.999596	0.000494	0.001136
2.800	5.178599	1.999771	0.000056	0.000490
3.200	5.978522	1.999847	0.000005	0.000172
3.600	6.778475	1.999924	0.000000	0.000042
4.000	7.578459	2.000000	0.000000	0.000000

Table 1 (b) : Numerical results using SOR Method and Simpson's(1/3) Rule for finer grid size

M=1.0, λ =2.0, P_r =1.0, n=1.0				
η	f	f'	θ	L
0.000	0.000000	1.000000	1.000000	0.000000
0.400	0.539397	1.617558	0.497618	0.005381
0.800	1.246713	1.877696	0.200941	0.005972
1.200	2.019285	1.967900	0.064629	0.004583
1.600	2.812649	1.993205	0.016249	0.002877
2.000	3.611355	1.998850	0.003144	0.001551
2.400	4.411150	1.999841	0.000462	0.000725
2.800	5.211123	1.999975	0.000051	0.000291
3.200	6.011117	1.999985	0.000004	0.000096
3.600	6.811112	1.999992	0.000000	0.000022
4.000	7.611110	2.000000	0.000000	0.000000

Table 2 (a) : Numerical results using SOR Method and Simpson's(1/3) Rule for finer grid size

M=5.0, λ=0.1, P_r =1.0, n=1.0				
η	f	f'	θ	L
0.000	0.000000	1.000000	1.000000	0.000000
0.400	0.270389	0.440437	0.699814	-0.004351
0.800	0.397231	0.227689	0.485287	-0.004972
1.200	0.469680	0.147457	0.327296	-0.004296
1.600	0.521690	0.117454	0.212888	-0.003305
2.000	0.566084	0.106337	0.132897	-0.002365
2.400	0.607668	0.102259	0.079194	-0.001594
2.800	0.648227	0.100783	0.044512	-0.001005
3.200	0.688418	0.100261	0.022729	-0.000571
3.600	0.728480	0.100078	0.009055	-0.000251
4.000	0.768493	0.100000	0.000000	0.000000

Table 2 (b) : Numerical results using SOR Method and Simpson's(1/3) Rule for finer grid size

M=20.0, λ=0.1, P_r =1.0, n=1.0				
η	f	f'	θ	L
0.000	0.000000	1.000000	1.000000	0.000000
0.400	0.207110	0.248932	0.659256	-0.002873
0.800	0.274684	0.124445	0.405422	-0.002358
1.200	0.319195	0.103973	0.228093	-0.001534
1.600	0.359924	0.100633	0.116829	-0.000906
2.000	0.400038	0.100091	0.054397	-0.000505
2.400	0.440052	0.100005	0.023020	-0.000270
2.800	0.480051	0.099993	0.008856	-0.000138
3.200	0.520048	0.099994	0.003085	-0.000066
3.600	0.560046	0.099997	0.000911	-0.000025
4.000	0.600045	0.100000	0.000000	0.000000

Table 3 (a) : Numerical results of f' on different grid sizes

M=0, λ=2.0, P_r =1, n=1				
η	h=0.05	h=0.025	h=0.012	Extrapolated
0.000	1.000000	1.000000	1.000000	1.000000
0.400	1.581951	1.581831	1.581453	1.581296
0.800	1.854353	1.854203	1.853704	1.853496
1.200	1.958560	1.958445	1.958062	1.957903
1.600	1.990561	1.990500	1.990268	1.990171
2.000	1.998316	1.998284	1.998135	1.998073
2.400	1.999774	1.999752	1.999596	1.999531
2.800	1.999981	1.999961	1.999771	1.999691
3.200	1.999998	1.999989	1.999847	1.999788
3.600	1.999998	1.999995	1.999924	1.999894
4.000	2.000000	2.000000	2.000000	2.000000

Table 3 (b) : Numerical results of f' on different grid sizes

M=0, λ=0.1, P_r =1, n=1				
η	h=0.05	h=0. 025	h=0.012	extrapolated
0.000	1.000000	1.000000	1.000000	1.000000
0.400	0.687636	0.687627	0.687590	0.687574
0.800	0.479185	0.479174	0.479101	0.479071
1.200	0.341249	0.341238	0.341152	0.341116
1.600	0.250843	0.250831	0.250743	0.250707
2.000	0.192189	0.192179	0.192097	0.192063
2.400	0.154522	0.154514	0.154449	0.154421
2.800	0.130563	0.130558	0.130512	0.130492
3.200	0.115446	0.115443	0.115416	0.115405
3.600	0.105956	0.105956	0.105944	0.105940
4.000	0.100000	0.100000	0.100000	0.100000

Table 4 (a): Numerical results of f' on different grid sizes

M=10, λ =2.0, P_r =1, n=1				
η	h=0.05	h=0.025	h=0.012	extrapolated
0.000	1.000000	1.000000	1.000000	1.000000
0.400	0.343772	0.343542	0.343483	0.343463
0.800	0.165492	0.165371	0.165337	0.165325
1.200	0.117448	0.117397	0.117380	0.117374
1.600	0.104606	0.104585	0.104575	0.104572
2.000	0.101202	0.101193	0.101186	0.101183
2.400	0.100309	0.100304	0.100301	0.100300
2.800	0.100077	0.100074	0.100073	0.100072
3.200	0.100018	0.100015	0.100016	0.100016
3.600	0.100004	0.100002	0.100003	0.100004
4.000	0.100000	0.100000	0.100000	0.100000

Table 4 (b): Numerical results of f' on different grid sizes

M=20, λ =0.1, P_r =1, n=1				
η	h=0.05	h=0. 025	h=0.012	extrapolated
0.000	1.000000	1.000000	1.000000	1.000000
0.400	0.249419	0.249031	0.248932	0.248898
0.800	0.124607	0.124481	0.124445	0.124433
1.200	0.104017	0.103986	0.103973	0.103969
1.600	0.100648	0.100641	0.100633	0.100630
2.000	0.100102	0.100100	0.100091	0.100087
2.400	0.100015	0.100014	0.100005	0.100001
2.800	0.100002	0.100001	0.099993	0.099989
3.200	0.100000	0.099999	0.099994	0.099991
3.600	0.100000	0.100000	0.099997	0.099995
4.000	0.100000	0.100000	0.100000	0.100000

Table 5: Results for $f''(0)$ for different values of M when, P_r =1.0, n=1.0

M	$\lambda = 2$		$\lambda = 0.1$	
	Micropolar Fluids (case-I)	Newtonian Fluids	Micropolar Fluids (case-I)	Newtonian Fluids
0.0	1.896296	1.9416628	-0.924357	-0.946575
1.0	2.101037	2.169651	-1.245284	-1.275179
5.0	2.740405	2.849281	-2.052678	-2.100383
10.0	3.360052	3.436086	-2.707299	-2.768844

Table 6: Comparison of the values of $f''(0)$ for Newtonian and micropolar fluids

Cases	$f''(0)$	
	$\lambda = 2.5$	$\lambda = 0.5$
Newtonian Fluid	4.386699	-1.221812
Micropolar Fluid(case-I)	4.287586	-1.193975
Micropolar Fluid(case-II)	2.801619	-0.776054
Micropolar Fluid(case-III)	1.987733	-0.550389

Table 7: $-\theta'(0)$ for different values of P_r , λ and n

P_r	$-\theta'(0)$	λ	$-\theta'(0)$	n	$-\theta'(0)$
0.5	0.612713	0.0	0.888150	-0.5	0.341769
1.0	0.928314	0.5	1.080513	0.0	0.566487
2.0	1.410216	1.0	1.227500	1.0	0.930866
5.0	2.362475	2.0	1.472164	2.0	1.226741
8.0	3.031640	4.0	1.861182	3.0	1.477719

Table 8: $-\theta'(0)$ for different values of λ and *M*

λ =2.0		λ =0.1		λ =0.5	
M	$-\theta'(0)$	M	$-\theta'(0)$	M	$-\theta'(0)$
0.0	0.3699684	0.0	0.2543771	0.0	0.2793221
1.0	0.3729475	1.0	0.2389634	1.0	0.2743733
5.0	0.3811157	5.0	0.2235448	5.0	0.2671146

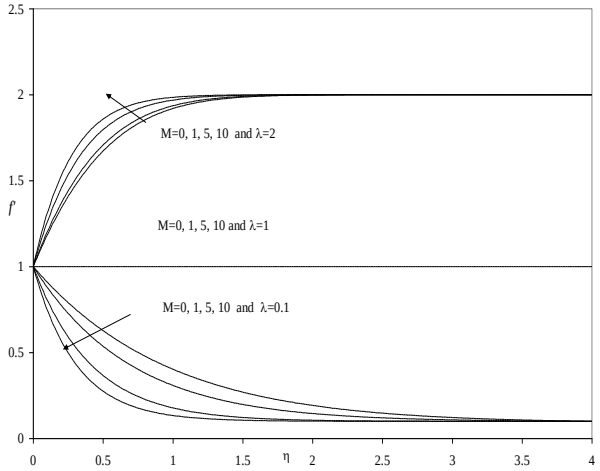

Fig.1: Graph of f' for different values of *M*.

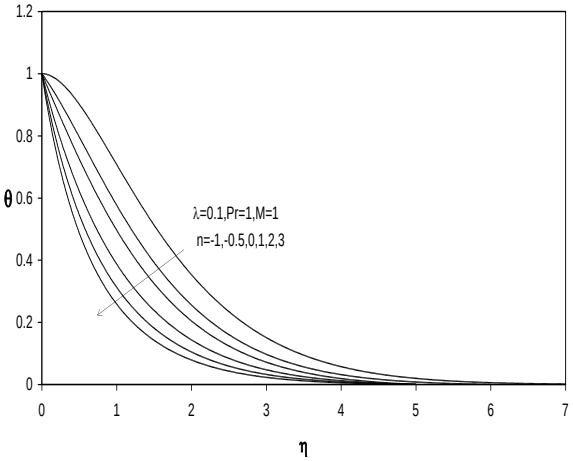

Fig.2: Graph of θ for different values of n

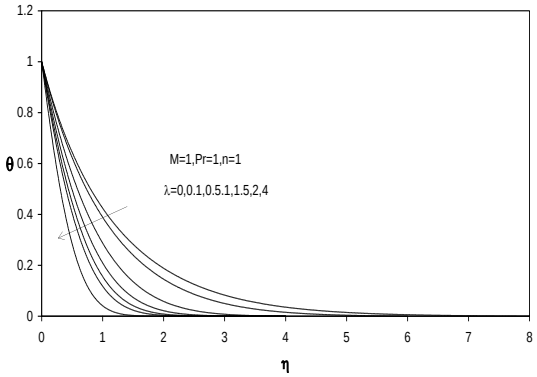

Fig.3: Graph of θ for different values of λ

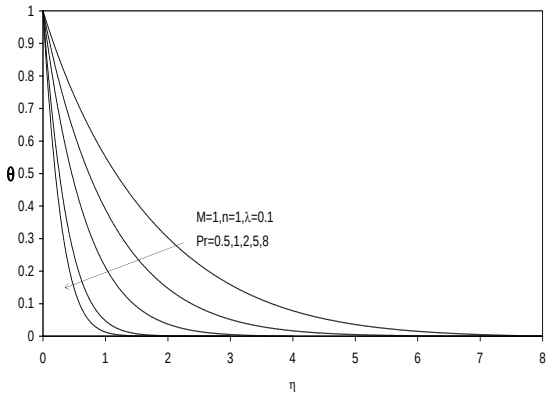

Fig .4: Graph of θ for different values of Pr when $\lambda = 0.1$

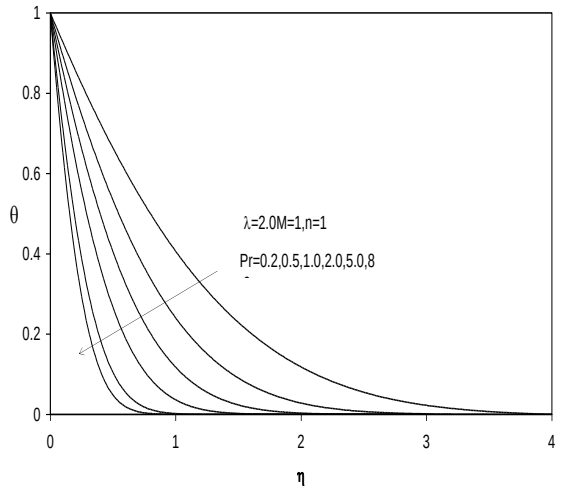

Fig .5: Graph of θ for different values of Pr when $\lambda = 2$.

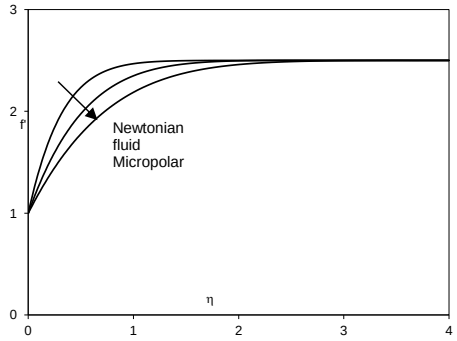

Fig.6: Graph of f' for comparison of Newtonian and Micropolar fluids when $\lambda = 2.5$, M=5.0, Pr =1.0, n=1.0

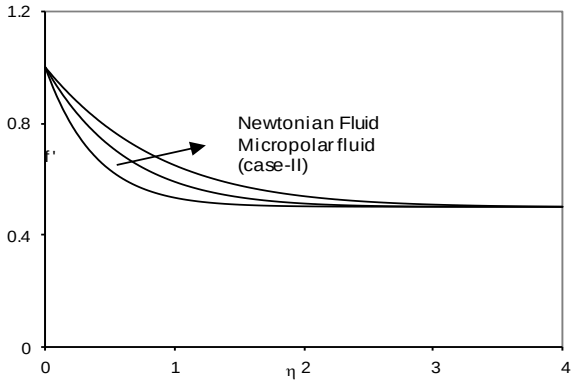

Fig .7: Graph of f' in comparison of Newtonian and Micropolar fluids when $\lambda = 0.5$, M=5.0, Pr =1.0, n=1.0

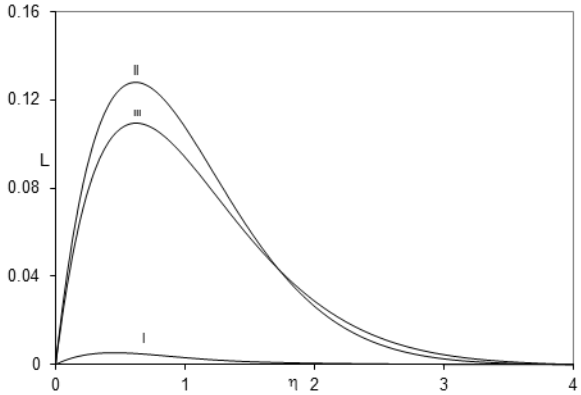

Fig.8: Graph of microrotation L for three cases: I, II, III of the non-dimensional constantswhen $\lambda = 2.5$, M=5.0, Pr=1.0, n=1.0

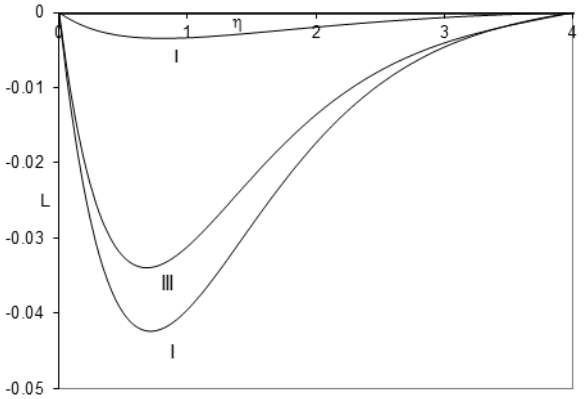

Fig.9: Graph of microrotation $L$for three cases: I, II, III of the non-dimensional constantswhen $\lambda = 0.5$, M=5.0, Pr=1.0, n=1.0

REFERENCES

[1] Eringen, A. C., Simple micro fluids, *Int J Eng Sci,2(2)*, 205-217(1964).

[2] Eringen, A. C., Theory of micropolar fluids, *J Math Mech*, 16(1),1-16(1966).

[3] Mahapatra, T. R., Gupta, A. S., Magnetohyderodynamic stagnation point flow towards a stretching sheet, *Acta Mechanica*, 152, 191-196 (2001).

[4] Seddeek, M. A., Flow of a magneto- micropolar fluid past a continuously moving plate. *Phys. Lett. A*, 306, 255-57(2003).

[5] Rehman, M. A., Rehman, A. A., Samad, M. A., Alam, M. A., Heat transfer in a micropolar fluid

along a non linear stretching sheet with a temperature- dependent viscosity and variable surface temperature, *Int. J. Thermo Phys*., 30, 649-670 (2009).

[6] Mohammadein, A. A., Gorla, R. S. R., Effects of transverse magnetic field on mixed convection in a micropolar fluid on a horizontal plate with vertical mass transfer. *Int. Numer. Meth. Heat Fluid Flow*, 11, 50(2001).

[7] Kamal, M.A., Hussain, S., Stretching a surface in a rotating micropolar fluid, *Int Journal of science and technology Spring Hall*, 30-36(1994).

[8] Lok, Y. Y., Pop, I., Chamkha, A., Non orthogonal stagnation point flow of a micropolar fluid, *Int. J. Engng. Sci.*, 45, 173-184(2007).

[9] Kumari, M., Nath, G., Unsteady self-similar stagnation point boundary layers for micropolar fluids, *Int. J. Eng. Sci.*, 22 :755(1984).

[10] Ashraf, M., Kamal, M.A., Syed, K.S., Numerical simulation of a micropolar fluid between a porous disk and a non- porous dis. *Appl. Math. Modell.*, 33,1933-1943 (2009).

[11] Ishak, A., Nazar, R., Pop, I., Mixed convection stagnation point flow of a micropolar fluid towards a stretching sheet, *Meccanica*, 43, 411-418(2008).

[12] Ishak, A., Jafar, K., Nazar, R., Pop, I., MHD stagnation point flow towards a stretching sheet. *Physica A*, 388: 3377-3383(2009).

[13] Smith, G.D., Numerical Solution of Partial Differential Equation. Clarendon Press: Oxford (1979).

[14] Gerald, C.F., Applied Numerical Analysis. Addison-Wesley Pub: NY (1989).

[15] Milne, W. E., Numerical Solution of Differential Equation. Dover Pub (1970).

[16] Burden, R.L., Numerical Analysis. Prindle Weber & Schmidt: Boston (1985).

[17] Ishak, A., Nazar, R., Pop, I., MHD flow of a micropolar fluid towards a stagnation point on a vertical surface, *Computers and Mathematics with Applications*, 56, 3188-3194(2008).

[18] Hayat, T., Abbas, Z., Pop, I., Asghar, S., Effects of radiation and magnetic field on the mixed convection stagnation-point flow. *International Journal of Heat and Mass Transfer*, 53, 466-474(2010).

[19] Hayat, T., Javed, T., Abbas, Z., MHD flow of a micropolar fluid near a stagnation point, *Nonlinear Analysis Real World Applications*, 10, 1514-1526(2009).

[20] Hussain, S., Kamal, M. A., Magnetohydrodynamic boundary layer micropolar fluid flow over a rotating disk. *International Journal of Computational and Applied Mathematics*, 7(3), 301-13(2012).

[21] Rossow, V. J., On flow of electrically conducting fluids over a flat plate in the presence of a transverse magnetic field. *Tech Report 1358, NASA*, 1958.